arXiv:cond-mat/9607100v1 15 Jul 1996

Full capacitance matrix of coupled quantum dot arrays: static and dynamical effects

C. B. Whan, J. White, and T. P. Orlando

Department of Electrical Engineering and Computer Science,

Massachusetts Institute of Technology, Cambridge, MA 02139

(February 1, 2008)

Abstract

We numerically calculated the full capacitance matrices for both one-dimensional (1D) and two-dimensional (2D) quantum-dot arrays. We found it is necessary to use the full capacitance matrix in modeling coupled quantum dot arrays due to weaker screening in these systems in comparison with arrays of normal metal tunnel junctions. The static soliton potential distributions in both 1D and 2D arrays are well approximated by the unscreened $(1/r)$ coulomb potential, instead of the exponential fall-off expected from the often used nearest neighbor approximation. The Coulomb potential approximation also provides a simple expression for the full inverse capacitance matrix of uniform quantum dot arrays. In terms of dynamics, we compare the current-voltage (I-V) characteristics of voltage biased 1D arrays using either the full capacitance matrix or its nearest neighbor approximation. The I-V curves show clear differences and the differences become more pronounced when larger arrays are considered.

Typeset using REVTEX

Much progress has been made in understanding the transport properties of single quantum dots [1]. In contrast, much less is known about transport through multiple quantum dots coupled by tunnel barriers. Recent experiments have mostly concentrated on double-dot or triple-dot systems [2–4], with the exception of Ref. [5] which is devoted to large two-dimensional (2D) quantum dot arrays. In analyzing quantum dot arrays, most authors [1,5,6] assume that in the classical charging regime (i.e. $\Delta E < k_B T \ll E_C$, where E_C is the charging energy of the dot and ΔE is the quantum energy level spacing), one can simply use the existing analysis for metal tunnel junction arrays [7–10]. The purpose of this letter is to explicitly demonstrate that even in the classical charging regime, an important distinction exists between quantum dot arrays in semiconductors and metal tunnel junction arrays, due to the difference in their abilities to screen electric charge.

In metal tunnel junction arrays [11], the junctions form very effective parallel plate capacitors due to the high dielectric constant of the barrier material (for example, in $Al/Al_2O_3/Al$ junctions, $\epsilon \approx 10\epsilon_0$ for the Al_2O_3 barrier) as well as the extremely small barrier thickness (~ 1 nm). As a consequence, the electrical potential due to an extra charge (the so-called soliton) placed on one of the metal islands in an array of tunnel junctions gets screened and decays rapidly with the distance away from the charged island. Until recently, most analyses [7–10] considered only the nearest neighbor junction capacitance C and the self-capacitance of the junction electrodes C_0 when constructing the capacitance matrix of the array. For a one-dimensional (1D) array, this approximation leads to an exponential decay of the soliton potential away from the center, with a characteristic screening length [7], $\lambda = a\sqrt{C/C_0}$, where a is the lattice constant of the array.

For quantum dot arrays made by electrostatic confinement of two-dimensional electron gas (2DEG) in GaAs/AlGaAs heterostructures [4], the array is a co-planar structure in which all the dots reside in the 2DEG plane. The co-planar capacitors are far less effective than the parallel plates in terms of confining electric field. Therefore, in comparison with tunnel junction arrays, the field lines originating from one of the quantum dots are much less confined and can reach out to dots that are much further apart. A model that considers

only the nearest neighbor capacitive coupling is unlikely to be accurate in this situation. We now give a more quantitative analysis of this problem.

In our model, the quantum dots (small puddles of a 2DEG) are treated as thin circular shaped conducting plates, with diameter $D = 1$ μm. The plates are arranged to form either 1D or 2D arrays with lattice constant $a \equiv D + d = 1.1$ μm, where $d = 0.1$ μm is the closest separation between adjacent dots (or the tunnel barrier width). We believe these values are reasonable for arrays in the classical charging regime with weak inter-dot tunneling (i.e. the tunneling resistance, $R_T \gg R_Q \equiv h/e^2$). Once the array geometry is specified, we compute the full capacitance matrix $\mathbf{C}$ of the 1D and 2D arrays using FASTCAP, an efficient capacitance extraction tool [12].

The inverse of the capacitance matrix gives us the potential distribution in the array for a given charge distribution within the array. In particular, the potential distribution due to a soliton (antisoliton) located at dot i in an $N \times 1$ array is given by,

$$\begin{pmatrix} \phi_1 \\ \vdots \\ \phi_i \\ \vdots \\ \phi_N \end{pmatrix} = \mathbf{P} \begin{pmatrix} 0 \\ \vdots \\ \pm e \\ \vdots \\ 0 \end{pmatrix}, \tag{1}$$

where, $\mathbf{P} \equiv \mathbf{C^{-1}}$, is the inverse of the capacitance matrix.

In Fig. 1a, we show the potential distribution due to a soliton located at the center ($i = 11$) of a 21×1 series array, using both the full capacitance matrix and its nearest neighbor approximation. The nearest neighbor approximation is obtained by setting all the non-nearest-neighbor off-diagonal elements to zero in the full capacitance matrix. As we can see, the nearest neighbor approximation gives an exponentially decaying soliton potential as expected [7]. However, the soliton potential distribution that we get from the full capacitance matrix decays much slower.

As we pointed out earlier, due to the spread-out nature of quantum dot arrays, there is

relatively weak screening of electrostatic potentials. Therefore we might expect the soliton potential distribution to follow the usual $1/r$ Coulomb potential at large distances. In Fig. 1b, we compare the full capacitance matrix soliton potential distribution with the Coulomb potential of a point charge e located at the soliton position. We see that the soliton potential follows the simple $1/r$ law almost exactly in the entire range, except at the origin where the Coulomb potential is singular.

In order to obtain an expression for the potential at the origin, $\phi_i(i)$, we recall that $\phi_i(i)$ is the electrical potential of dot i when a unit charge is placed on it and all the other dots are left neutral. When a dot has charge Q and is isolated in free space, its electrical potential will be, $\phi_0 = Q/C_0$, where C_0 is the self-capacitance of an isolated dot. From simple dimensional analysis, we expect C_0 to have the form, $C_0 = \alpha\pi\epsilon_0 D$, for a dot with diameter D. Using FASTCAP, we determine the numerical factor $\alpha \approx 1.23$. When other (neutral) conductors are brought nearby, it should not disturb the potential ϕ_0 too much and therefore we take, $\phi_i(i) \approx e/C_0$. Thus, we have the following approximate expression for the soliton potential distribution in a 1D quantum dot array:

$$\phi_j(i) = \begin{cases} \frac{e}{\alpha\pi\epsilon_0 D} & \text{if } i = j; \\ \frac{e}{4\pi\epsilon_0 a}\frac{1}{|i-j|} & \text{if } i \neq j. \end{cases} \tag{2}$$

The results from Eq. (2) are denoted by the cross (+) symbols in Fig. 1b.

Recently, Likharev and Matsuoka [13] pointed out that even in tunnel junction arrays, the nearest neighbor approximation is questionable. By considering full capacitance matrices of tunnel junction arrays and comparing them with an analytical continuum model, they proposed a phenomenological formula for the soliton potential distribution in 1D tunnel junction arrays. We attempted to fit our results to their formula, the best fit gives essentially the same result as the simple Coulomb potential, except at the the origin their formula overestimates $\phi_i(i)$ by roughly a factor of 2. This is not surprising since their formula was obtained for tunnel junction arrays where $\lambda \gg a$. In our quantum dot arrays, however, the opposite limit, $\lambda < a$, applies.

We also carried out similar calculations for 2D arrays of quantum dots. In Fig. 2, we plot the soliton potential distribution in a 11×11 array with the soliton located in the center, using both the full capacitance matrix and its nearest neighbor approximation. Again, we found that the soliton potential in the nearest neighbor approximation follows the expected form [8,10], $\phi(r) \propto e^{-r/\lambda}/\sqrt{r}$ for $\lambda < a$ (not shown in the figure). The 2D soliton potential, when full capacitance matrix is considered, is once again well-approximated by the simple formula

$$\phi(x,y) = \begin{cases} \frac{e}{\alpha\pi\epsilon_0 D} & \text{if } x = y = 0 \\ \frac{e}{4\pi\epsilon_0}\frac{1}{\sqrt{x^2+y^2}} & \text{otherwise,} \end{cases} \tag{3}$$

assuming the soliton is located at the origin of the coordinate system.

According to Eq. (1), if we know the potential distributions for all possible soliton locations, we can determine the full inverse capacitance matrix. Therefore, for 1D and 2D uniform disk-shaped quantum dot arrays, we can approximately write down the inverse capacitance matrix, $\mathbf{P}$, without any numerical calculations [see Eqs. (2), and (3)]:

$$\mathbf{P}_{ij} = \begin{cases} \frac{1}{\alpha\pi\epsilon_0 D} & \text{if } i = j; \\ \frac{1}{4\pi\epsilon_0}\frac{1}{|\mathbf{r}_i - \mathbf{r}_j|} & \text{if } i \neq j. \end{cases} \tag{4}$$

So far, our analysis assumes that our array is in free space (or in a uniform dielectric medium if we make the substitution $\epsilon_0 \rightarrow \epsilon$). In reality, the 2DEG plane is buried in a dielectric medium with $\epsilon \approx 13\epsilon_0$, very close to ($\sim 300$ Å) the sample surface. Underneath the 2DEG, the same dielectric medium continues over the entire sample thickness (including the GaAs substrate, which is about 0.5 mm thick). Therefore in a more realistic model for a quantum dot array, we can treat the array as being located at the interface between the free space (ϵ_0) and an infinitely thick substrate with permittivity $\epsilon = 13\epsilon_0$. We can calculate the capacitance matrix of this system using FASTCAP assisted by the static image method. The result amounts to making the simple substitution, $\epsilon_0 \rightarrow \epsilon/2$, in the above analysis.

Having shown that the the full capacitance matrix is needed to model the static soliton potential in quantum dot arrays, we now briefly address the effect of full capacitance matrix

on dynamical properties. In particular, we compute the current-voltage (I-V) characteristics of voltage biased arrays using Monte Carlo method [7–9]. In Fig. 3, we compare I-V curves for a 21×1 array computed using the full capacitance matrix and the nearest neighbor approximation. As we can see in Fig. 3, the two I-V curves clearly show many differences. The threshold voltages are not exactly the same, and the fine structures are different and they become more pronounced if we consider larger arrays. At high voltage, the two curves merge and become nearly linear, as shown in the inset of Fig. 3. The detailed analysis of the I-V curves, as well as some of the relevant numerical techniques, will be the subject of a future publication. Nevertheless, we see that the full capacitance matrix is necessary in the dynamical simulation of these arrays.

We acknowledge fruitful discussions with David Carter and Joel Phillips. This project is supported by NSF grant DMR-9402020, AFOSR grant F49620-95-1-0311, and ARPA Contract N00174-93-C-0035.

REFERENCES

[1] For a recent review see, L. P. Kouwenhoven and P. L. McEuen, in *Nano-Science and Technology*, edited by G. Tim (to be published by AIP Press, New York, 1996).

[2] M. Kemerink and L. W. Molenkamp, Appl. Phys. Lett. **65**, 1012 (1994).

[3] T. Sakamoto, S. Hwang, F. Nihey, Y. Nakamura, and K. Nakamura, Jpn. J. Appl. Phys. **33**, 4876 (1994).

[4] F. R. Waugh, M. J. Berry, D. J. Mar, R. M. Westervelt, K. L. Campman, and A. C. Gossard, Phys. Rev. Lett. **75**, 705 (1995).

[5] C. I. Duruöz, R. M. Clarke, C. M. Marcus, and J. S. Harris, Jr., Phys. Rev. Lett. **74**, 3237 (1995).

[6] A. A. Middleton and N. S. Wingreen, Phys. Rev. Lett. **71**, 3198 (1993).

[7] N. S. Bakhvalov, G. S. Kazacha, K. K. Likharev, and S. I. Serdyukova, Zh. Eksp. Theor. Fiz. **95**, 1010 (1989) [Sov. Phys. JETP **68**, 581 (1989)].

[8] N. S. Bakhvalov, G. S. Kazacha, K. K. Likharev, and S. I. Serdyukova, Physica (Amsterdam) **173B**, 319 (1991).

[9] U. Geigenmüller and G. Schön, Europhys. Lett. **10**, 765 (1989).

[10] J. E. Mooij, B. J. van Wees, L. J. Geerligs, M. Peters, R. Fazio, and G. Schön, Phys. Rev. Lett. **65**, 645 (1990).

[11] P. Delsing, in *Single Charge Tunneling*, edited by H. Grabert and M. H. Devoret (Plenum, New York, 1992).

[12] K. Nabor, S. Kim, and J. White, IEEE Trans. Microwave Theory Tech. **40**, 1496 (1992).

[13] K. K. Likharev and K. A. Matsuoka, Appl. Phys. Lett. **67**, 3037 (1995).

FIGURES

FIG. 1. (a) The potential distribution due to a soliton located at the center ($i = 11$) of a 21×1 array. The circular symbol corresponds to the full capacitance matrix calculation and the square is for nearest neighbor approximation. The inset is a sketch of one section of our array. (b) The soliton potential distribution from the full capacitance matrix calculations (circles) compared with the predictions of Eq. (2)(crosses).

FIG. 2. The soliton potential distributions in a 11×11 2D array of quantum dots, using the full capacitance matrix (solid line mesh) and the nearest neighbor approximation (dashed line mesh). The soliton is located at the center of the array ($x = y = 0$).

FIG. 3. Current-voltage characteristics of a 21×1 quantum dot array using, the full capacitance matrix (solid line) and the nearest neighbor approximation (dashed line). The inset shows the I-V at a larger scale.

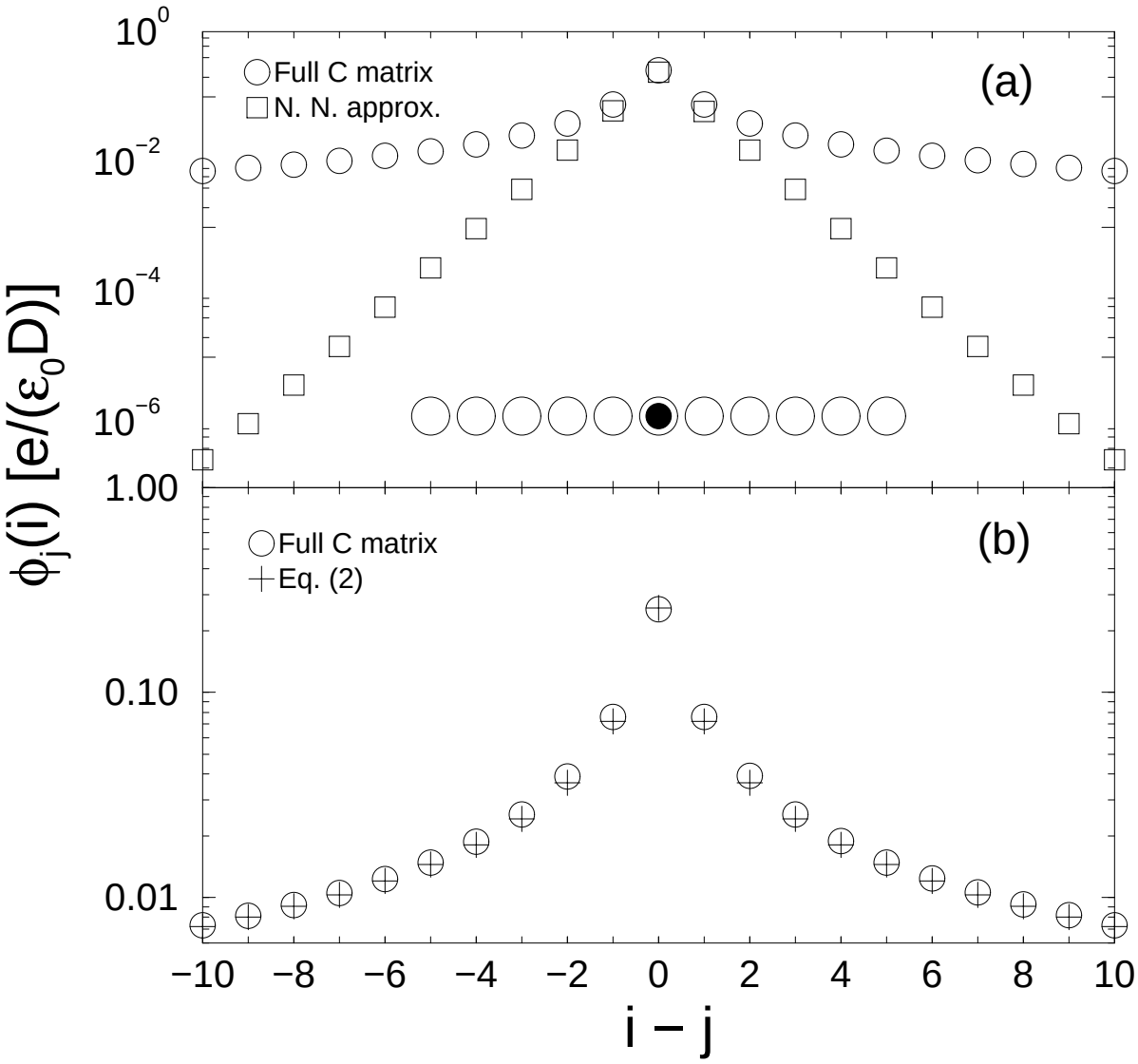
Full C matrix
N. N. approx.
(a)
Full C matrix
Eq. (2)
(b)
$\phi_j(i)$ [e/(ε_0D)]
i − j

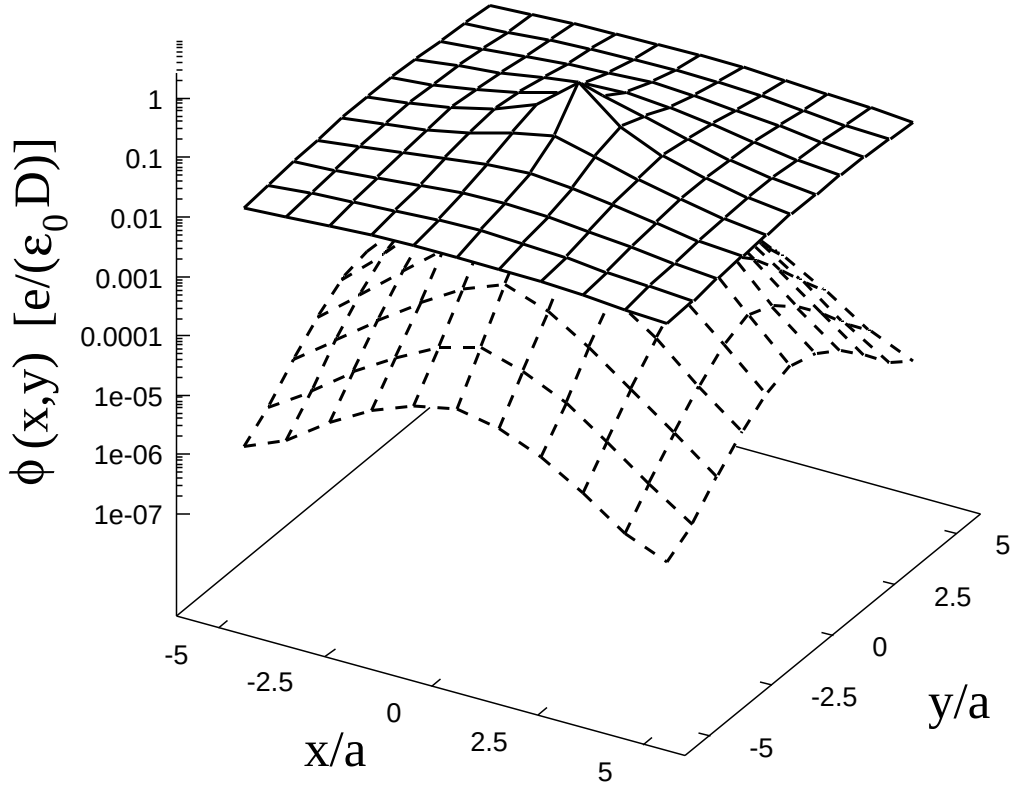
$\phi(x,y)$ [e/(ε_0 D)]
1
0.1
0.01
0.001
0.0001
1e-05
1e-06
1e-07
-5
-2.5
0
2.5
5
x/a
-5
-2.5
0
2.5
5
y/a

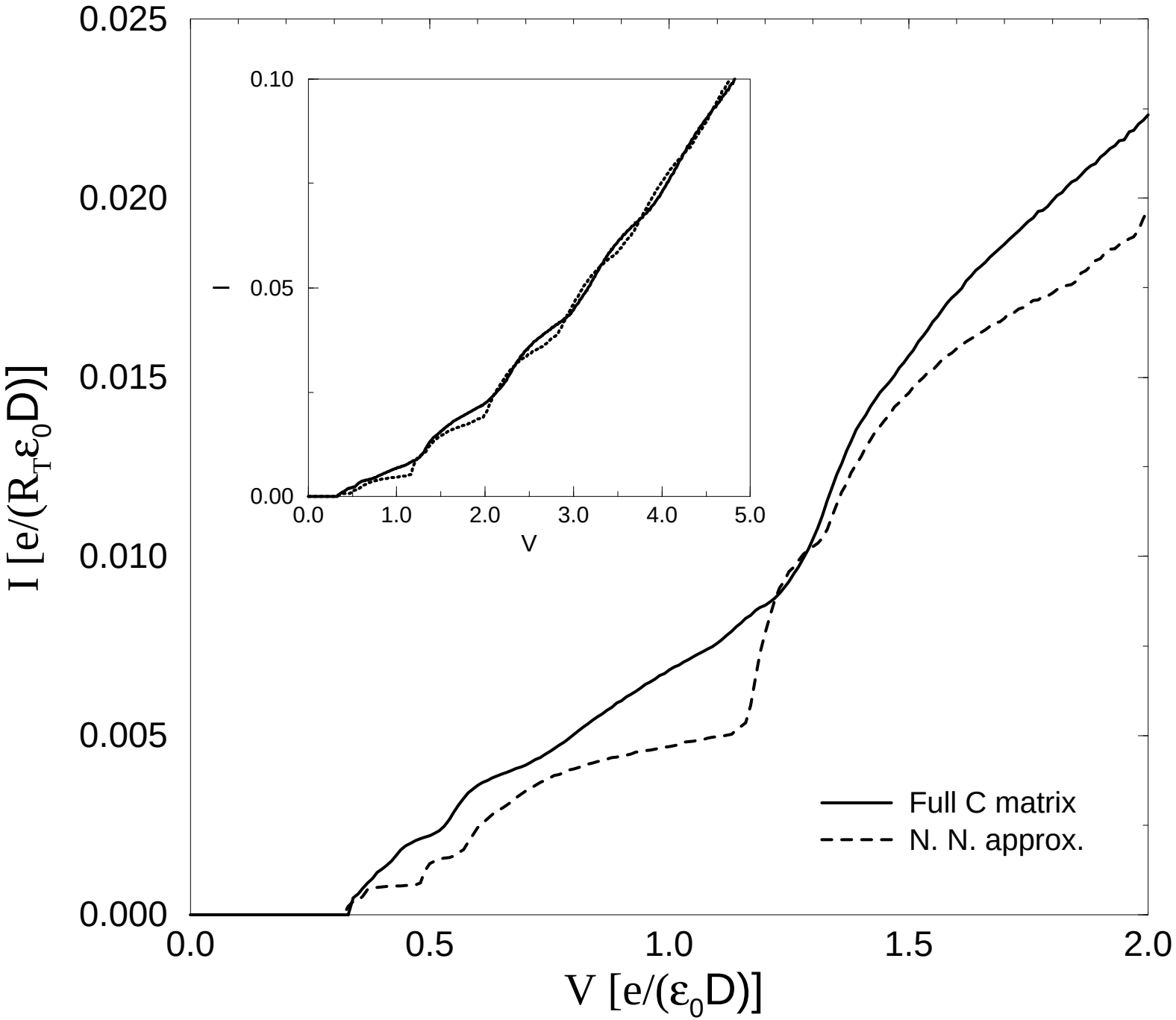

Whan et. al Fig.3